Full dimension Rb2He ground triplet potential energy surface and quantum scattering calculations

Grégoire Guillon, Alexandra Viel, Jean-Michel Launay

Full dimension Rb2He ground triplet potential energy surface and quantum scattering calculations

Grégoire Guillon, Alexandra Viel, and Jean-Michel Launay

Citation: The Journal of Chemical Physics **136**, 174307 (2012); doi: 10.1063/1.4709433
View online: http://dx.doi.org/10.1063/1.4709433
View Table of Contents: http://scitation.aip.org/content/aip/journal/jcp/136/17?ver=pdfcov
Published by the AIP Publishing

Full dimension Rb_2He ground triplet potential energy surface and quantum scattering calculations

Grégoire Guillon,[a] Alexandra Viel,[b] and Jean-Michel Launay[c]
Institut de Physique de Rennes, UMR 6251, CNRS & Université de Rennes 1, F-35042 Rennes, France

(Received 20 February 2012; accepted 16 April 2012; published online 3 May 2012)

We have developed a three-dimensional potential energy surface for the lowest triplet state of the Rb_2He complex. A global analytic fit is provided as in the supplementary material [see supplementary material at http://dx.doi.org/10.1063/1.4709433 for the corresponding Fortran code]. This surface is used to perform quantum scattering calculations of ^{4}He and ^{3}He colliding with $^{87}Rb_2$ in the partial wave $J = 0$ at low and ultralow energies. For the heavier helium isotope, the computed vibrational relaxation probabilities show a broad and strong shape resonance for a collisional energy of 0.15 K and a narrow Feshbach resonance at about 17 K for all initial Rb_2 vibrational states studied. The broad resonance corresponds to an efficient relaxation mechanism that does not occur when ^{3}He is the colliding partner. The Feshbach resonance observed at higher collisional energy is robust with respect to the isotopic substitution. However, its effect on the vibrational relaxation mechanism is faint for both isotopes. © *2012 American Institute of Physics*. [http://dx.doi.org/10.1063/1.4709433]

I. INTRODUCTION

An always increasing interest in producing dense samples of cold molecules has been registered during the last years. The highly remarked success in cooling atomic gases to quantum degeneracy as well as the resulting new physics have prompted many efforts worldwide to cool molecular gases to similarly cold temperatures. Indeed, quantum gases of tightly bound molecules can be used to investigate ultracold reactions or collisions between molecules, to produce molecular Bose-Einstein condensates and to develop molecular quantum optics by trapping them in optical lattices.

Rubidium appears to be one of the most popular atoms in the cold physics community especially since its use for the first demonstration of Bose-Einstein condensation in a dilute medium.[1] Unfortunately, standard laser cooling techniques as developed for atoms are not efficient for molecules due to their complex internal structure. Other ways to produce cold and dense molecular samples are thus required. Direct methods such as Stark or Zeeman deceleration[2] and sympathetic cooling[3] have already been proposed. Indirect techniques that involve pre-cooled atoms, such as photoassociation[4] or association via magnetically tuned Feshbach resonances[5] have also been considered.

The first observation of translationally cold rubidium molecules was reported in 2000 by the Pisa and Florence groups for both ^{85}Rb and ^{87}Rb isotopes at a temperature of about 90 μK.[6] These dimers were produced in the radiatively stable $^3\Sigma_u^+$ triplet ground state by a photoassociation technique using a magneto-optical trap. In the same experiment, $^{85}Rb_2$ cold molecules were also directly produced during the trap operation alone by three-body recombination.[7–9]

In 2003,[10,11] quantum degenerate or nearly degenerate ultracold molecular gases have been produced by association via Feshbach resonances.[5] In this case, the molecules were produced in very weakly bound states corresponding to large vibrational quantum numbers. Since then, the production of dense samples of deeply bound molecules has been performed by various optical schemes. In particular, a dense ensemble of $^{87}Rb_2$ molecules has been produced more recently in a single quantum level of the rovibrational ground state of the Rb_2 triplet potential $a^3\Sigma_u^+$.[12]

Rubidium dimers in their ground triplet state $^3\Sigma_u^+$ have been formed on the surface of helium droplets more than 10 years ago.[13] High spin alkali dimers are selectively produced[13,14] because the binding energy that is released when two rubidium atoms collide on the droplet is smaller for the high spin state than for the low spin state, for which a significant evaporation of the droplet occurs. Rubidium dimers are now extensively studied both in Graz[15–18] and in Freiburg.[19–21] The vibrational dynamics of Rb_2 attached on the surface of He_n droplets has been recently studied by a femtosecond pump-probe technique.[20,21] A model using a dissipative quantum approach has been proposed in Ref. 21 that allows the interpretation of the femtosecond experiments as a vibrational relaxation induced dephasing mechanism.

A two-dimensional potential energy surface for a rigid Rb_2 molecule ($^3\Sigma_u^+$) interacting with a helium atom has been recently proposed in Ref. 22. It was used to study the structure and the energetics as well as the rotational dynamics of Rb_2 treated as a rigid dimer attached to small ^{4}He clusters and films. However, the fixed Rb_2 distance of the surface prohibits its usage for the study of vibrational dynamics. We thus report in Sec. II a full dimensional potential energy surface for the ground triplet state of the Rb_2He complex. This global three-dimensional surface is then used in Sec. III for quantum scattering calculations of the vibrational relaxation mechanism. While all the various isotope combinations are of

[a]Present address: Department of Chemistry, University of Waterloo, Waterloo, Ontario N2L 3G1, Canada.
[b]Electronic mail: alexandra.viel@univ-rennes1.fr.
[c]Electronic mail: jean-michel.launay@univ-rennes1.fr.

interest, only ^{4}He and ^{3}He colliding with a $^{87}Rb_2$ dimer have been considered here. We have considered an energy domain which ranges from ultralow to low temperatures and which covers, in particular, the temperatures relevant to ^{3}He and ^{4}He nanodroplets (respectively, 150 mK and 380 mK). The hyperfine structure has not been taken into account and only the $J = 0$ partial wave has been considered.

II. FULL-DIMENSIONAL INTERACTION POTENTIAL

A. Electronic structure calculations

We have performed *ab initio* calculations of the first triplet state $1^3A'$ of the Rb_2He molecule as explained in a previous work.[22] We have used the MOLPRO 2010.1 package[23] to perform restricted Hartree–Fock calculations followed by a determination of the energies at the single-reference restricted open-shell coupled cluster method with single, double, and non-iterative triple excitations. The nine valence electrons ($4s^2 4p^6 5s$) of each rubidium atom and the two electrons of the helium atom are treated dynamically. We used the basis set referred as **B** in Ref. 24 for the description of the valence electrons of the rubidium atoms and the uncontracted d-aug-cc-pV5Z basis set for the description of the helium atom. The inner electrons of the rubidium atoms were described using the ECP28MDF relativistic core potential.[25]

The resulting well depth for Rb_2 is $D_e = 323.6$ K (including the counterpoise correction) for a distance of 6.118 Å.[26] At this *ab initio* level, the HeRb diatomic potential presents an equilibrium distance of 7.42 Å and a well depth of 1.34 K. The well depth obtained is in good agreement with the 1.4 K value obtained by recent *ab initio* computations[27] but substantially smaller than the 2.1 K value proposed by Pascale.[28] The most stable geometry of the triatomic Rb_2He system is a T-shape one with the He atom lying at a distance of 6.3 Å from the Rb_2 center of mass and the Rb_2 internuclear distance equal to 6.1 Å.

B. Analytical fit of the potential energy surface

The full potential representation is based on the following many-body decomposition:[29]

$$V(R,\gamma,r) = V^{1B} + V^{2B}_{RbHe}(R_1) + V^{2B}_{RbHe}(R_2) + V^{2B}_{RbRb}(r) + V^{3B}(R,\gamma,r), \quad (1)$$

where R_1, R_2, and r correspond, respectively, to the two RbHe and to the Rb_2 distances, while R, γ, r are the Jacobi coordinates. R is the distance between the helium atom and the Rb_2 center of mass. In our notation, $\gamma = 0$ corresponds to linear geometry, while $\gamma = \pi/2$ corresponds to the T-shape configuration. The two-body (2B) and the three-body (3B) terms are fitted using the reproducing kernel Hilbert space (RKHS) interpolation method of Ho and Rabitz.[30]

For the Rb_2 and RbHe diatomic potentials, we used an expansion in reproducing kernels $q_1^{3,2}(x,x')$ as defined in Ref. 30, x being the square of the interatomic distances R_1, R_2, or r,

$$q_1^{3,2}(x,x') = \frac{0.3}{x_>^3}\left(1 - \frac{x_<}{x_>} + \frac{2}{7}\frac{x_<^2}{x_>^2}\right), \quad (2)$$

TABLE I. Long-range coefficients taken from Ref. 32 for RbHe and from Refs. 33 and 34 for Rb_2.

	Rb_2	RbHe
C_6 [$E_h\, a_0^6$]	4.707×10^3	4.469×10^1
C_8 [$E_h\, a_0^8$]	5.730×10^5	3.145×10^3
C_{10} [$E_h a_0^{10}$]	7.665×10^7	3.038×10^5

where $x_> = \max(x,x')$ and $x_< = \min(x,x')$. The choice of this reproducing kernel ensures a $-C_6/R^6 - C_8/R^8 - C_{10}/R^{10}$ long-range behavior.[31] We used 27 *ab initio* points ranging from 1 Å to 50 Å for RbHe and 26 *ab initio* points ranging from 2 Å to 50 Å for Rb_2. For distances larger than 50 Å the resulting diatomic potentials agree with the C_6, C_8, and C_{10} expansion obtained from published coefficients given in Table I to better than 0.5% for RbHe and 3% for Rb_2. For RbHe, a 2004 work[35] updated the C_6 value to a slightly lower 43.4 $E_h\, a_0^6$ value.

For the three-body term, we used 1584 *ab initio* points sampling a three-dimensional (R, γ, r) grid with six angles $\gamma = 0°$, 15°, 30°, 45°, 67.5°, and 90°, 22 R distances ranging from 5.0 to 30.0 Å, and 12 r distances ranging from 4.0 to 9.0 Å. The grid mesh was denser in the region of the potential well, that is, in the neighborhood of the values $r = 6.1$ Å and $R = 6.30$ Å. We employed an expansion over products of three low order one-dimensional reproducing kernels $\tilde{q}_2^1(x_1,x_1')\tilde{q}_2^1(x_2,x_2')q_2^1(x_3,x_3')$ with

$$x_1 = \exp(-a_1 R), \quad (3a)$$

$$x_2 = \exp(-a_2 r), \quad (3b)$$

$$x_3 = \sin\gamma, \quad (3c)$$

and

$$\tilde{q}_2^1(x,x') = \min(x,x'), \quad (4a)$$

$$q_2^1(x,x') = 1 + \min(x,x'), \quad (4b)$$

as defined in Refs. 30 and 36. In Eqs. (3), the x_1 and x_2 variables have been chosen as decreasing exponentials in R and r as suggested in Ref. 37 to account for the rapid decrease of V_{3B} at large R and r. A value of 0.4 for both a_1 and a_2 has been found to be suitable. This expansion allows a faithful representation of the three-body term in the regions of configuration space which are relevant to the scattering calculations presented below. Given the small polarizability of He, the Axilrod-Teller-Muto long-range term[38] is not considered explicitly in the potential. The FORTRAN subroutine to evaluate the full potential, Eq. (1), is provided: see supplementary material in Ref. 39 for the FORTRAN source code of the potential surface.

We have paid attention to employ consistent *ab initio* energies especially in the asymptotic part, while computing the RKHS expansion coefficients. In particular, care has been taken when correcting from the basis set superposition errors (BSSE), for which the original counterpoise (CP)

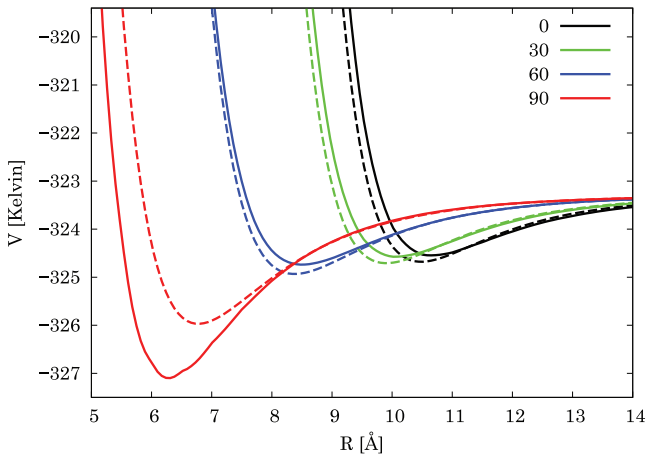

FIG. 1. Cuts of the potential energy surface at $r = 6.117$ Å for $\gamma = 0°$ (black), 30° (green), 60° (blue), and $\gamma = 90°$ (red) in Kelvin as a function of R. The full potential surface is presented in full lines while the restriction to the two-body expansion is shown in dashed lines. The zero of energy corresponds to the separated atoms limit.

correction of Boys and Bernardi[40] has been used. In the case of complexes with more than two atoms, different valid ways of implementing the CP correction are possible. They differ in the path that is followed to form the complex from the constituting atoms. Although the overall binding energy should be independent of the chosen path, corrected interaction energies may be different.[41,42] In this work, we implemented the CP procedure in the most symmetrical and less ambiguous way, namely, it is applied to the interaction energy associated with the complex formation $Rb_a + Rb_b + He \rightarrow Rb_2He$, with the use of the trimer basis for all separated He, Rb_a, and Rb_b atomic fragments. Aware of some arguments that the counterpoise procedure could over-correct for BSSE, we maintained its usage for the computation of corrected energies. This choice is motivated by the detailed analysis of Gutowski,[43] Cybulski,[44] and van Duijneveldt,[45,46] showing that this procedure is rigorously correct, and by the fact that for very weakly bound van der Waals complexes, the comparison of theoretical and experimental values shows the superiority of the counterpoise corrected energies.[47]

C. Potential energy surface

The resulting global surface has a T-shape minimum which occurs at a distance He–Rb of 6.986 Å and a distance Rb–Rb of 6.114 Å, in good agreement with the geometry of the minimum at the *ab initio* level. The corresponding potential value, −327.103 K, is 3.826 K below the He + Rb_2 dissociation limit. Figure 1 presents one-dimensional cuts of the potential surface and underlines the contribution of the three-body term.

The effect of the three-body term is most noticeable at distances around the potential well and below where it brings a small attractive contribution for perpendicular configurations and a tiny repulsive contribution for linear configurations.

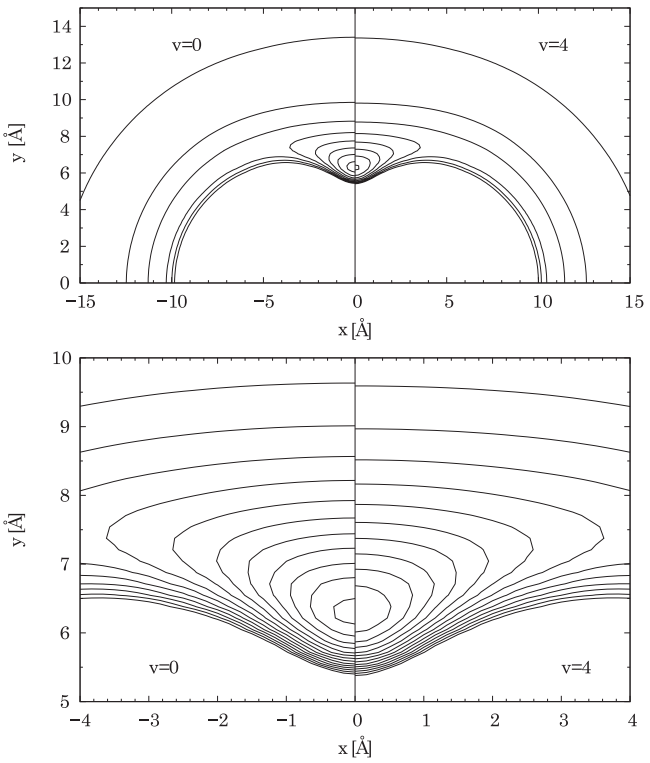

FIG. 2. Contour plots of potential energy surfaces averaged over the $v = 0$ (left panels) and the $v = 4$ (right panels) vibrational states of Rb_2. The helium atom is localized by its Cartesian coordinates assuming that Rb_2 lies along the x axis. The contour lines are with respect to the He + Rb_2 dissociation limit. The contour line spacing is 0.5 K for the upper panel and 0.3 K for the lower panel which focuses on the potential well region.

Two-dimensional cuts of the potential surface averaged over the $v = 0$ and $v = 4$ vibrational wavefunctions of Rb_2 are presented in Fig. 2. These plots are only slightly affected by the average over the Rb_2 vibrational motion whose amplitude is 0.50 Å for $v = 0$ and 1.53 Å for $v = 4$. Contour lines for $v = 4$ are less dense, which shows that the effective potential well felt by the helium atom is shallower when the Rb_2 vibration amplitude increases.

III. QUANTUM SCATTERING CALCULATIONS

Quantum calculations of the elastic and inelastic He + $Rb_2(v_i, j_i) \rightarrow$ He + $Rb_2(v_f, j_f)$ collision for total angular momentum $J = 0$ have been performed with a time-independent close coupling approach. We have used a modified version of the MOLCOL computer code[48] in which the treatment of vibrational excitation has been improved. The coupled equations have been solved using the Johnson-Manolopoulos[49] log-derivative propagator. We have considered the heavier isotope of the rubidium dimer $^{87}Rb_2$ and both ^{4}He and ^{3}He isotopes. The resulting Rb_2 rotational constant is 0.0148 K and the $v = 0 \rightarrow v = 1$ excitation energy is 18.223 K. Eighteen even j rotational levels of the vibrational $v = 0$ ground state lie below the $(v = 1, j = 0)$ level. Rovibrational states of Rb_2 with vibrational quantum number up to 5 and even rotational states with j up to 48 have been used in the close-coupling expansion. A propagation range from 4 to 60 Å ensures probabilities which are converged with

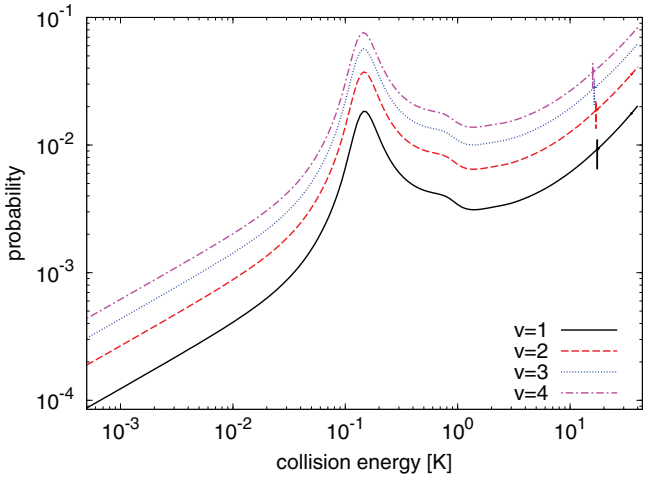

FIG. 3. Vibrational relaxation probability for ^{4}He as a function of the collision energy in Kelvin for initial rovibrational states $(v_i, j = 0)$ with $v_i = 1, 2, 3$, and 4.

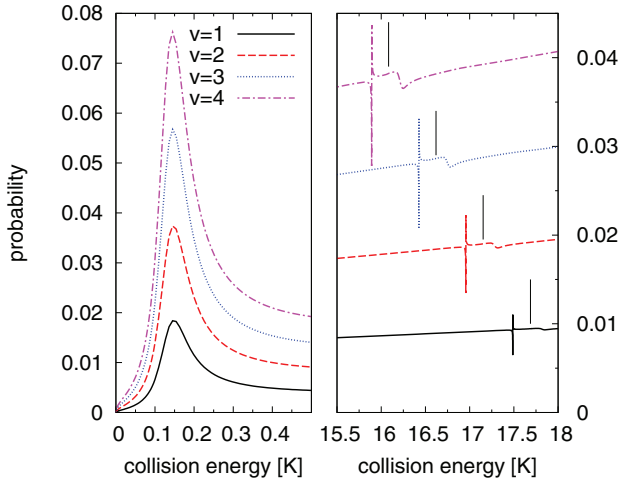

FIG. 4. Vibrational relaxation probability for ^{4}He as a function of collision energy in Kelvin for initial rovibrational states $(v_i, j_i = 0)$ with $v_i = 1, 2, 3$, and 4. This figure presents two blow-ups of the data presented in Fig. 3 in the energy ranges of the two resonance features. The openings of the $(v_i + 1, j = 0)$ channels are materialized by the vertical black lines in the right panel.

graphical accuracy. Runs at ultralow collision energies have been performed with an extended range up to 500 Å to evaluate scattering lengths.

Figure 3 shows vibrational relaxation probabilities $\sum_f |T_{if}|^2$ for several initial excited rovibrational states $(v_i, j_i = 0)$ and final rovibrational states (v_f, j_f) with $v_f < v_i$. These probabilities increase almost proportionally to the v_i quantum number and have contributions arising predominantly from $\Delta v = -1$ transitions. This predominance of the $\Delta v = -1$ transitions was already noticed in a study on He + H_2 scattering.[50] At low collisional energy, the probabilities follow the Wigner law for $\ell = 0$ scattering and are proportional to the square root of the collision energy. All curves in Fig. 3 present a strong and broad resonant feature around 0.145 K and a faint and very narrow one around 17 K.

Figure 4 focuses on these two energy ranges. First a very large increase of the relaxation probability occurs at 0.145 K for all v_i. This resonance constitutes an efficient relaxation mechanism. The position and the width of this low energy shape resonance depends only very slightly on v_i. It shifts slightly towards lower collisional energies when v_i increases in agreement with the already mentioned observation that the effective potential is slightly less attractive as the Rb_2 vibrational excitation increases. Second, we see a very narrow resonant feature around 17 K. It lies systematically 0.2 K below the openings of the $(v_i + 1, j = 0)$ channels. This feature disappears when the $v_i + 1$ manifold is not included in the close-coupling calculations and can thus be classified as a Feshbach resonance. In a previous study,[22] it was found that ^{4}He is bound to a rigid $^{85}Rb_2$ molecule by 0.193 K, a value which is in reasonable agreement with the position of this resonance. Figure 4 shows also that the relaxation probability decreases slightly after the opening of the $v_i + 1$ manifold. This decrease is due to a broad resonance in the $v_i \rightarrow v_i + 1$ excitation probability. Due to the anharmonicity of the Rb_2 potential, all these features shift systematically towards smaller collision energy as v_i increases.

Figure 5 shows the changes of the vibrational relaxation probability with respect to the ^{4}He → ^{3}He isotopic substitution. We can see on the left panel that the relaxation probability obtained with ^{3}He at 0.15 K is decreased by a factor of 20 and is no longer a maximum but a minimum. We see on the right panel that the second resonance is still present but its position and detailed shape are modified. The dispersion profile obtained with ^{3}He is inverted with respect to the one obtained with ^{4}He. The resonance occurs at a larger collision energy but stays below the opening the of $v_i + 1$ manifold. This shift towards higher energies is consistent with a larger zero point energy of the quasi-bound state with the lighter isotope. The zero point energy of the quasi-bound state should be understood here as the zero point energy of bound states of Rb_2He when Rb_2 is restricted to be in the $v = 2$ vibrational state.

Figure 5 shows also the effect of the three-body term of the interaction potential by comparing the vibrational

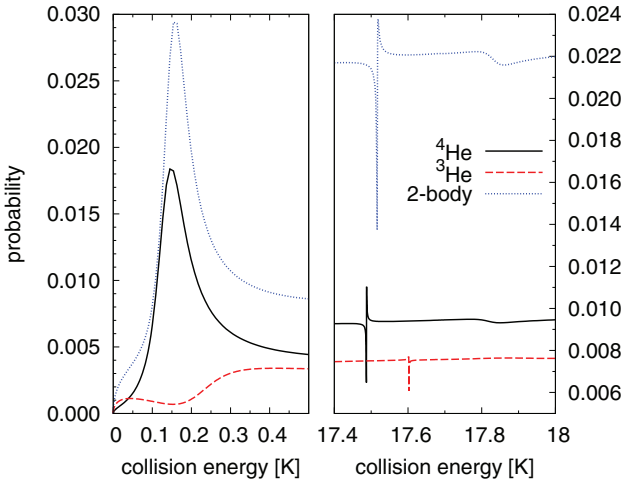

FIG. 5. Vibrational relaxation probability for $v_i = 1$ as a function of collision energy in K. The black full line corresponds to ^{4}He colliding with Rb_2 using the full potential. The red dashed line presents the effect of the isotopic substitution of ^{4}He by ^{3}He on the full potential. The blue pointed line is obtained when ^{4}He collides with Rb_2 on the two-body potential surface.

relaxation probability obtained with the full potential and with the two-body potential only. The resonances are still present when the three-body term is removed but their positions are shifted to higher collision energy by about 0.01 K for the low energy one, and 0.03 K for the other one. The three-body term deepens the minimum of the potential seen in Fig. 1 by about 1 K, while for linear configuration it renders the potential more repulsive. The shift of the resonance positions towards lower energies when the three-body term is added shows that on average the interaction potential is slightly more attractive. This is coherent with Ref. 22 where it was shown that the bound state of the Rb_2–He complex presents a very delocalized wavefunction which samples all angular geometries. Finally, the profile of the 0.145 K resonance is not changed, while the one of the 17 K resonance is slightly affected by the three-body term.

Figure 6 presents the elastic and inelastic rate coefficients restricted to the partial wave $J = 0$ for Rb_2 $(v_i, j_i = 0) + {}^4He$ scattering.

These are defined by

$$K_E = \frac{\pi\hbar}{mk_i}|T_{ii}|^2, \tag{5a}$$

$$K_I = \frac{\pi\hbar}{mk_i}(1 - |S_{ii}|^2), \tag{5b}$$

where i stands for (v_i, j_i), k_i is the wavevector, and m is the He + Rb_2 reduced mass. In the inelastic rate K_I, transitions corresponding to both vibrational relaxation and rovibrational excitation are included. The elastic rate coefficients for $1 \leq v_i \leq 4$ are graphically identical to the $v_i = 0$ curve and are thus not presented. We see that for energies smaller than 10^{-2} K, K_E and K_I follow Wigner threshold laws: K_I is constant and K_E increases as $\sqrt{E_{coll}}$. Contrarily to the case of the alkali-alkali dimer collisions Na + Na_2,[51] Li + Li_2,[52] and K + K_2,[53] the inelastic rate is smaller than the elastic one except at ultralow energies (10^{-7} K). Figure 6 also shows a very sharp increase of K_I which is accompanied by a drop in K_E above 0.02 K. These two features are due to the opening of the rotational state $j_f = 2$ which absorbs a large part of the incoming flux.

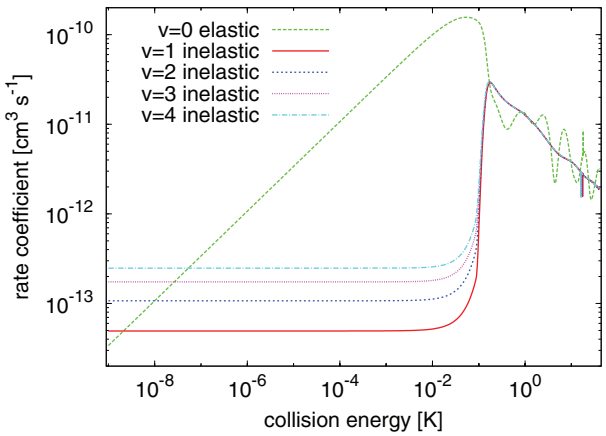

FIG. 6. Elastic and inelastic $J = 0$ rate coefficients for ${}^4He + Rb_2$ collisions with the initial rovibrational state $v_i = 0, \ldots, 4, j = 0$ of Rb_2 as a function of the collisional energy in Kelvin.

TABLE II. Scattering length as defined in Eq. (6) for ${}^4He$ and ${}^3He$ colliding with Rb_2 in various vibrational states $(v_i, j_i = 0)$. Values obtained when the three-body term of the potential is removed are also presented (2B).

Isotope	v_i	a(Å)
${}^4He$	0	11.33
${}^4He$	1	11.44
${}^4He$	2	11.53
${}^4He$	3	11.63
${}^4He$	4	11.73
${}^3He$	0	18.40
${}^3He$	1	18.51
${}^4He$ (2B)	0	13.33
${}^4He$ (2B)	1	13.35

For energies larger than 0.1 K, K_I decreases almost linearly with $1/E_{coll}$ and K_E presents Ramsauer-Townsend oscillations. K_E and K_I have comparable average values. This can be simply explained by a small value of the S-matrix element $|S_{ii}| \simeq 0.3$ resulting in both $\sum_{f \neq i}|S_{if}|^2 \simeq 0.9$ and $|T_{ii}|^2$ ranging from $(1 - 0.3)^2 = 0.5$ to $(1 + 0.3)^2 = 1.7$. K_I is found to be almost independent of the initial vibrational state because the potential energy surface depends very slightly on the Rb_2 distance.

Table II shows the real part of the scattering lengths for different initial rovibrational states.

These are defined by

$$a_i = \lim_{k_i \to 0} \Re \left\{ \frac{T_{ii}}{2ik_i} \right\}. \tag{6}$$

We find that a_i increases with v_i thus in agreement with a less attractive averaged interaction potential as the vibrational excitation increases. The variations of a_i when ${}^3He$ is considered as well as when the three-body term of the interaction potential is removed indicate also a less attractive potential on average. This is consistent with the variation of the position of the second resonance towards a larger collision energy in these two cases (see Fig. 5). An analysis of the variation of a for the $(v_i = 0, j_i = 0)$ ground rovibrational level when the reduced mass varies from the one for ${}^4He$ to the one for ${}^3He$ shows no divergence. This indicates that the $Rb_2{}^3He$ complex has only one bound state as $Rb_2{}^4He$ for $J = 0$.[22] At low collision energy both K_I and K_E are larger with ${}^3He$ than with ${}^4He$. With ${}^3He$, K_I is above K_E below 3.04 nanoK, while this occurs below 2.02 nanoK for ${}^4He$.

Figure 7 presents the rotational distributions of the $(v_i = 1, j_i = 0) \rightarrow (v_f = 0, j_f)$ transition for three collisional energies, 10^{-6} K, 0.15 K, and 2 K. We see that they depend rather strongly both on the colliding partner and on the energy. In the ${}^4He$ case, there is a strong $j_f/2$ even or odd alternation at $E_{coll} = 10^{-6}$ K. This behavior does not occur for the lighter isotope. At the resonance energy (panel (b)), both $j_f = 2$ and $j_f = 4$ contribute in the ${}^4He$ case while we see a depletion for the $j_f = 2$ level with ${}^3He$. The rotational distributions do not show any general behavior as underlined by the large differences obtained when performing the isotopic substitution. These distributions contrast with the one of He

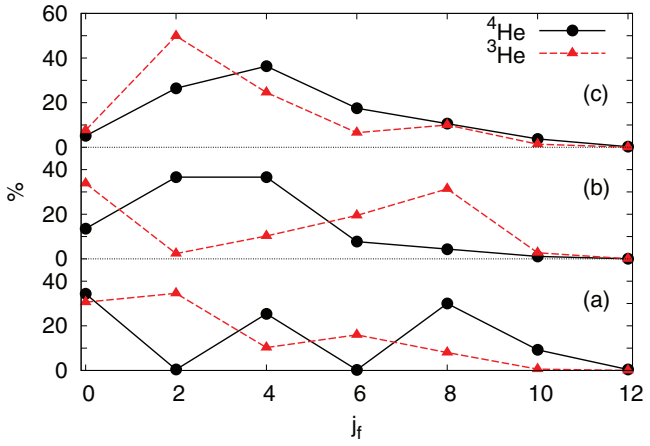

FIG. 7. Rotational distribution of the $(v_i = 1, j_i = 0) \rightarrow (v_f = 0, j_f)$ transition for three collision energies, (a) 10^{-6} K, (b) 0.15 K, and (c) 2 K for both ^{4}He (black circles) and ^{3}He (red triangle).

+ CaH at low energy scattering for which bimodal distributions have been found.[54]

IV. CONCLUSION

In this work, we have presented a preliminary study of the vibrational deactivation of $^{87}Rb_2$ in its ground triplet state induced by collisions with both helium isotopes ^{4}He and ^{3}He in the cold and ultracold regimes. We have built a new and accurate three-dimensional potential energy surface to describe the triatomic system, interpolated from an extensive set of *ab initio* energies. The rubidium core electrons have been modeled by a recent effective potential which has proven to reproduce faithfully spectroscopic data at the atomic level.

Quantum calculations restricted to the total angular momentum $J = 0$ have been performed on this potential energy surface for vibrationally excited $^{87}Rb_2$ colliding with one helium atom. In this system, the Wigner regime is reached for collision energies below 0.01 K. Above 0.1 K, inelastic probabilities have been found independent of the initial vibrational state of $^{87}Rb_2$ consistently with a weak vibrational coupling in the Rb_2He complex. Test calculations which include only two-body interactions show that the location and shape of the resonance features are slightly affected by the three-body term of the potential surface. Finally, we have shown the existence of only one bound state of the Rb_2He complex for both He isotopes for $J = 0$.

A limitation of our present work is the absence of hyperfine, spin-spin, and spin-rotation terms in the Rb_2 molecule. However, the detailed spectroscopic analysis of $^{87}Rb_2$ in the lowest triplet state[55] has shown their importance. Work dedicated to assess the role of these terms in the collisional observables is currently in progress in our group together with $J \neq 0$ computations. On another line of research, the present three-dimensional surface will enable to describe the vibrational relaxation mechanism of $a^3\Sigma_u^+$ Rb_2 dimers adsorbed on helium droplets and films along an approach similar to the one which is proposed in Ref. 56.

ACKNOWLEDGMENTS

This work is supported by the Région Bretagne via the project CREATE "4023-HELIUM" and by the "DYN-HELIUM" ANR project. Pavel Soldán is warmfully thanked for fruitful discussions.

[1] M. H. Anderson, J. R. Ensher, M. R. Matthews, C. E. Wieman, and E. A. Cornell, Science **269**, 198 (1995).
[2] S. Y. T. van de Meerakker, H. L. Bethlem, and G. Meijer, Nat. Phys. **4**, 595 (2008).
[3] J. Doyle, B. Friedrich, R. Krems, and F. Masnou-Seeuws, Eur. Phys. J. D **31**, 149 (2004).
[4] K. M. Jones, E. Tiesinga, P. D. Lett, and P. S. Julienne, Rev. Mod. Phys. **78**, 483 (2006).
[5] T. Köhler, K. Góral, and P. S. Julienne, Rev. Mod. Phys. **78**, 1311 (2006).
[6] C. Gabbanini, A. Fioretti, A. Lucchesini, S. Gozzini, and M. Mazzoni, Phys. Rev. Lett. **84**, 2814 (2000).
[7] A. J. Moerdijk, H. M. J. M. Boesten, and B. J. Verhaar, Phys. Rev. A **53**, 916 (1996).
[8] P. O. Fedichev, M. W. Reynolds, and G. V. Shlyapnikov, Phys. Rev. Lett. **77**, 2921 (1996).
[9] A. Leggett, Rev. Mod. Phys. **73**, 307 (2001).
[10] J. Herbig, T. Kraemer, M. Mark, T. Weber, C. Chin, H.-C. Nägerl, and R. Grimm, Science **301**, 1510 (2003).
[11] S. Jochim, M. Bartenstein, A. Altmeyer, G. Hendl, S. Riedl, C. Chin, J. H. Denschlag, and R. Grimm, Science **302**, 2101 (2003).
[12] F. Lang, K. Winkler, C. Strauss, R. Grimm, and J. H. Denschlag, Phys. Rev. Lett. **101**, 133005 (2008).
[13] F. R. Brühl, R. A. Miron, and W. E. Ernst, J. Chem. Phys. **115**, 10275 (2001).
[14] J. Higgins, C. Callegari, J. Reho, F. Stienkemeier, W. E. Ernst, M. Gutowski, and G. Scoles, J. Phys. Chem. A **102**, 4952 (1998).
[15] O. Allard, J. Nagl, G. Auböck, C. Callegari, and W. E. Ernst, J. Phys. B **39**, S1169 (2006).
[16] G. Auböck, J. Nagl, C. Callegari, and W. E. Ernst, J. Phys. Chem. A **111**, 7404 (2007).
[17] G. Auböck, M. Aymar, O. Dulieu, and W. E. Ernst, J. Chem. Phys. **132**, 054304 (2010).
[18] M. Theisen, F. Lackner, and W. E. Ernst, J. Phys. Chem. A **115**, 7005 (2011).
[19] C. P. Schulz, P. Claas, D. Schumacher, and F. Stienkemeier, Phys. Rev. Lett. **92**, 013401 (2004).
[20] M. Mudrich, P. Heister, T. Hippler, C. Giese, O. Dulieu, and F. Stienkemeier, Phys. Rev. A **80**, 042512 (2009).
[21] B. Grüner, M. Schlesinger, P. Heister, W. T. Strunz, F. Stienkemeier, and M. Mudrich, Phys. Chem. Chem. Phys. **13**, 6816 (2011).
[22] G. Guillon, A. Zanchet, M. Leino, A. Viel, and R. E. Zillich, J. Phys. Chem. A **115**, 6918 (2011).
[23] H.-J. Werner, P. J. Knowles, G. Knizia, F. R. Manby, M. Schütz *et al.*, MOLPRO, version 2010.1, a package of *ab initio* programs, 2010, see http://www.molpro.net.
[24] P. Soldán, J. Chem. Phys. **132**, 234308 (2010).
[25] I. S. Lim, P. Schwerdtfeger, B. Metz, and H. Stoll, J. Chem. Phys. **122**, 104103 (2005).
[26] Note that a typo is present in Ref. 22. We cite the well depth of the scaled diatomic curve of Ref. 24 and not the *ab initio* value as it should be.
[27] T. V. Tscherbul, P. Zhang, H. R. Sadeghpour, and A. Dalgarno, Phys. Rev. A **79**, 062707 (2009).
[28] J. Pascale, "Service de Physique des Atomes et des Surfaces," Technical Report, CEN Saclay, Gif sur Yvette, France, October 1983.
[29] J. N. Murrell and S. Carter, J. Phys. Chem. **88**, 4887 (1984).
[30] T. S. Ho and H. Rabitz, J. Chem. Phys. **104**, 2584 (1996).
[31] P. Soldán and J. M. Hutson, J. Chem. Phys. **112**, 4415 (2000).
[32] J. Mitroy and M. W. J. Bromley, Phys. Rev. A **68**, 062710 (2003).
[33] A. Marte, T. Volz, J. Schuster, S. Dürr, G. Rempe, E. G. M. van Kempen, and B. J. Verhaar, Phys. Rev. Lett. **89**, 283202 (2002).
[34] M. Marinescu, H. R. Sadeghpour, and A. Dalgarno, Phys. Rev. A **49**, 982 (1994).
[35] C. Zhu, A. Dalgarno, S. G. Porsev, and A. Derevianko, Phys. Rev. A **70**, 032722 (2004).
[36] T. S. Ho, T. Hollebeek, H. Rabitz, L. B. Harding, and G. C. Schatz, J. Chem. Phys. **105**, 10473 (1996).

[37]A. Zanchet, B. Bussery-Honvault, and P. Honvault, J. Phys. Chem. A **110**, 12017 (2006).
[38]B. M. Axilrod and E. Teller, J. Chem. Phys. **11**, 299 (1943).
[39]See supplementary material at http://dx.doi.org/10.1063/1.4709433 for the Fortran source code.
[40]S. F. Boys and F. Bernardi, Mol. Phys. **19**, 553 (1970).
[41]B. H. Wells and S. Wilson, Chem. Phys. Lett. **101**, 429 (1983).
[42]L. Turi and J. J. Dannenberg, J. Phys. Chem. **97**, 2488 (1993).
[43]M. Gutowski, J. H. Van Lenthe, J. Verbeek, F. Van Duijneveldt, and G. Chałasinski, Chem. Phys. Lett. **124**, 370 (1988).
[44]S. M. Cybulski and G. Chałasinski, Chem. Phys. Lett. **197**, 591 (1992).
[45]G. Chałasinski and M. M. Szczesniak, Chem. Rev. **94**, 1723 (1994).
[46]F. B. Van Duijneveldt, J. G. C. M. Van Duijneveldt-van de Rijdt, and J. H. van Lenthe, Chem. Rev. **94**, 1873 (1994).
[47]E. G. Hohenstein, H. M. Jaeger, E. J. Carrell, G. S. Tschumper, and C. D. Sherril, J. Chem. Theory Comput. **7**, 2842 (2011).
[48]D. R. Flower, G. Bourhis, and J.-M. Launay, Comput. Phys. Commmun. **131**, 187 (2000).
[49]D. E. Manolopoulos, J. Chem. Phys. **85**, 6425 (1986).
[50]N. Balakrishnan, R. C. Forrey, and A. Dalgarno, Phys. Rev. Lett. **80**, 3224 (1998).
[51]P. Soldán, M. T. Cvitaš, J. M. Hutson, P. Honvault, and J.-M. Launay, Phys. Rev. Lett. **89**, 153201 (2002).
[52]G. Quéméner, J.-M. Launay, and P. Honvault, Phys. Rev. A **75**, 050701 (2007).
[53]G. Quéméner, P. Honvault, J.-M. Launay, P. Soldán, D. E. Potter, and J. M. Hutson, Phys. Rev. A **71**, 032722 (2005).
[54]N. Balakrishnan, G. C. Groenenboom, R. V. Krems, and A. Dalgarno, J. Chem. Phys. **118**, 7386 (2003).
[55]C. Strauss, T. Takekoshi, F. Lang, K. Winkler, R. Grimm, J. H. Denschlag, and E. Tiemann, Phys. Rev. A **82**, 052514 (2010).
[56]R. E. Zillich and K. B. Whaley, Phys. Rev. B **69**, 104517 (2004).